

Persistent Freshening of the Arctic Ocean and Changes in the North Atlantic Salinity Caused by Arctic Sea Ice Decline

Hui Li (✉ hui7@ucar.edu)

National Center for Atmospheric Research <https://orcid.org/0000-0001-8242-5202>

Alexey Fedorov

Yale University

Research Article

Keywords: Arctic sea ice, Arctic freshwater content, Arctic climate, Atlantic Meridional Overturning Circulation, Climate change

Posted Date: June 16th, 2021

DOI: <https://doi.org/10.21203/rs.3.rs-584527/v1>

License:   This work is licensed under a Creative Commons Attribution 4.0 International License.

[Read Full License](#)

Abstract

Arctic sea ice has been declining over past several decades with the largest ice loss occurring in summer. This implies a strengthening of the sea ice seasonal cycle. Here, we examine global ocean salinity response to such changes of Arctic sea ice using simulations wherein we impose a radiative heat imbalance at the sea ice surface, inducing a sea ice decline comparable to the observed. The imposed perturbation leads to enhanced seasonal melting and a rapid retreat of Arctic sea ice within the first 5-10 years. We then observe a gradual freshening of the upper Arctic ocean that continues for about a century. The freshening is most pronounced within the central Arctic, including the Beaufort gyre, and is attributed to excess surface freshwater associated with the stronger seasonal sea ice melting, as well as a greater upper-ocean freshwater storage due to changes in ocean circulation. The freshening of the Nordic Seas can also occur via a distillation-like process in which denser saline waters with increased salinity are exported to the subtropical/tropical North Atlantic by meridional overturning circulation. Thus, enhanced seasonal sea ice melting in a warmer climate can lead to a persistent Arctic freshening with large impacts on the global salinity distribution.

1. Introduction

A critical component of the Earth's climate, the Arctic ocean responds quickly to global warming. Arctic sea ice has been declining at an unprecedented rate over the past three decades - since the 1980s, annual mean sea ice extent has decreased by about 20% (Stroeve et al. 2007; Cavalieri and Parkinson 2008; Kwok and Rothrock 2009). The changes are especially dramatic in summer as September sea ice extent and volume declined by about 30% and 60%, respectively (Eisenman et al. 2011; Goldstein et al. 2018) (Fig. 1d, e). The rapid loss of sea ice exerts profound impacts on the global climate through positive feedbacks that amplify global warming (i.e., Winton 2006; M. Serreze et al. 2009) and connections with mid-to-low latitudes (Cohen et al. 2014; Deser et al. 2015; Blackport and Kushner 2016; Liu et al. 2018; Wang et al. 2018a; Sun et al. 2018).

Recent observations show a gradual increase in the Arctic ocean freshwater content. Using salinity profiles from ships and autonomous drifting buoys, Rabe et al. (2014) reports that the liquid freshwater content of the upper Arctic basins has been increasing with a trend of $600 \pm 300 \text{ km}^3 \text{ yr}^{-1}$ over the period of 1992–2012. Several studies estimate that the accumulation of liquid freshwater in the Arctic during the 2000s may have resulted from unbalanced freshwater fluxes, changes of the Arctic Oscillation (Johnson et al. 2018; Cornish et al. 2020) and increased sea ice loss, though some uncertainties remain (Serreze et al. 2006; Bamber et al. 2012; Woodgate et al. 2012; Haine et al. 2015; Wang et al. 2018b). While the mechanisms of this ongoing Arctic freshening remain under debate, on multidecadal timescales the low salinity anomalies can potentially escape the Arctic and affect ocean deep convection sites in the subpolar North Atlantic, weakening the Atlantic Meridional Overturning Circulation (AMOC) (Scinocca et al. 2009; Oudar et al. 2017; Sévellec, Fedorov, and Liu 2017; Liu, Fedorov, and Sévellec 2018; Liu and Fedorov 2019). Therefore, as sea ice plays a central role in regulating surface freshwater input and more generally the hydrological cycle of polar regions (Aagaard and Carmack 1989), the question of

Arctic freshening and its relationship to sea ice decline becomes critical for ocean global circulation. Accordingly, the goal of this study is to investigate Arctic sea ice decline as a mechanism for the current and future Arctic freshening.

As we will show, using fully coupled climate simulations wherein we impose a sea ice decline comparable to the observed by creating a positive radiation imbalance over the ice (see Sect. 2), average salinity in the Arctic region (area north of 60°N) responds gradually but robustly to the imposed changes. We find that when the ocean reaches a new equilibrium after a century, the magnitude of the resultant Arctic ocean freshening exceeds the transient freshening due to the initial sea ice melting by nearly a factor of 3!

What causes this strong and persistent freshening of the Arctic? Here, we highlight the role of the enhanced sea ice seasonal cycle – the cycle of ice melting in summer and water refreezing and brine rejection in winter. Melting of sea ice adds freshwater to the surface layers, strengthening upper ocean stratification. Freezing of sea ice, on the other hand, expels most of the salt into the underlying ocean layer via brine rejection. The loss of sea ice can also affect the Arctic ocean freshwater distribution by modifying ocean circulation. In particular, the strengthening of the Beaufort gyre can increase freshwater storage in the Arctic (i.e., Proshutinsky et al., 2009). In addition, sea ice reduction and changes in sea ice seasonal melting impact the spatial distributions of freshwater fluxes, affecting the vertical salinity distribution and possibly deep convection. In turn, the excess salt in the deep ocean layer can be removed from the Arctic by the meridional overturning circulation. Thus, changes in the sea ice seasonal cycle can profoundly influence the upper-ocean salinity. These are the topics to be discussed in more detail in the next sections.

2. Models And Experiments

We use the fully coupled Community Earth System Model (CESM) version 1.1.2 developed at National Center for Atmospheric Research (NCAR). The detailed model configuration used in this study is documented in Liu et al. (2018). Here we emphasize some key aspects. The atmosphere component is the Community Atmosphere Model version 4 (CAM4) (Neale et al. 2012) with T31 horizontal resolution (~3.75° grid spacing). The ocean model is the Parallel Ocean Program version 2 (POP2) (Smith et al. 2010) on a nominal 3° horizontal resolution and has 60 vertical levels. Ocean latitudinal resolution increases to 0.5° near the equator and in high latitudes. The sea ice component of the model is the Community Ice Code, version 4 (CICE4) (Holland et al. 2012), sharing the same horizontal grid with the ocean component. Sea ice albedo is computed using parameter representing optical properties of snow, bare sea ice, and melt ponds where the parameters are based on standard deviations from data provided by the Surface Heat Budget of the Arctic (SHEBA) (Uttal et al. 2002). Our analysis is largely based on this climate model, to which we refer as the low-res model. We also compare the results to these simulations with those obtained from a different configuration of CESM1 that has a higher resolution.

Sea ice surface radiative balance is altered by either reducing sea ice surface albedo to increase shortwave absorption (named “SW” experiment) or reducing the sea ice surface emissivity to restrain outgoing long wave radiative fluxes (named “LW” experiment). In the SW experiment, we modify the optical properties of snow, bare sea ice, and ponded ice over the Arctic area within the model’s sea ice component. Specifically, we reduce the single scattering albedo of snow (the probability that a single event results in scattering) by 10% for all spectral bands and adjust the optical properties of bare ice and ponded ice by changing the standard deviation parameters from 0 to -2. For the LW experiment, we reduce the emissivity of snow and ice by a factor of 10^{-4} over the Arctic Ocean.

The SW and LW experiments are able to replicate the seasonality of the observed sea ice area reduction, which is stronger in summer and weaker in winter (Fig. 1d). These two experiments have 10 ensemble members each. Two additional experiments are also conducted with stronger shortwave absorption (“strong-SW”) and weaker longwave emission (“weak-LW”). All simulations start from a quasi-equilibrium preindustrial control climate. Sea ice perturbations are initiated from the beginning of each simulation and maintained for 200 years. The magnitude of maximum sea ice reduction is roughly proportional to the strength of sea ice radiative perturbations.

We focus in detail on the SW experiment. While the induced reduction in sea ice cover in SW is comparable to the observed over the past three decades, the reduction of sea ice volume is $\sim 2.8 \times 10^4$ km³, which is greater than the observation-based estimate of $\sim 1.4 \times 10^4$ km³. This is in large part because we use a preindustrial simulation as the control, and also because of the bias in sea ice thickness (too thick sea ice) common in climate models. It is also possible that the model is somewhat oversensitive to the disturbance specified. Despite the bias in sea ice thickness, our conclusions are still robust, as evidenced by the persistent freshening in the “weak-LW” experiment where the sea ice volume reduction is $\sim 1.2 \times 10^4$ km³.

For comparison, we also conduct experiments with a higher-resolution climate model. Specifically, we employ the f19_gx1v6 configuration of CESM1, in which the atmosphere model (CAM4) has $\sim 2^\circ$ horizontal resolution, and the ocean model (POP2) uses a nominal 1° horizontal resolution. The higher-resolution experiment uses a similar perturbation approach as the low-resolution SW experiment. We conducted three experiments with slightly different albedo modifications, where the optical properties of bare sea ice, and ponded ice are changed from 0 to -3, -4, and -5, respectively. The three experiments produced very similar sea ice decline that is generally consistent with the low-res SW experiment (supplementary Fig. S1). We regard these experiments as a small ensemble, while for brevity refer to this model as the high-res model.

Model results are also compared to the observations. The observational record for sea ice area is provided by the National Snow and Ice Data Center (NSIDC) and is based on gridded brightness temperatures from the Defense Meteorological Satellite Program (DMSP) series of passive microwave radiometers: the Special Sensor Microwave Imager (SSM/I) and the Special Sensor Microwave Imager/Sounder (SSM/IS). Sea ice volume is from Pan-Arctic Ice Ocean Modeling and Assimilation

System (PIOMAS) developed at APL/PSC (Zhang and Rothrock 2003; Schweiger et al. 2011). In PIOMAS, total sea ice volume only accounts for the region poleward of 65°N and area with sea ice thickness exceeding 0.15 m. We apply the same criteria to calculate the modeled total sea ice volume to maintain consistency.

3. Results

3.1 Upper ocean freshening in response to sea ice melting

Using the low-res model, we conduct four experiments that differ in either the type of radiative perturbation applied or the strength of the modified radiative fluxes. We analyze in more detail the shortwave (SW) experiment, in which sea ice surface albedo is reduced due to increased shortwave absorption.

In response to the imposed perturbations, annual mean sea ice and volume decrease rapidly in all experiments within the first 5–10 years and then remain fairly steady for the rest of the simulation (Fig. 1a, b). Sea ice volume decreases in all seasons, with a larger reduction in late summer (e.g., 70% in summer and 40% in winter in the SW experiment, Fig. 1e). The amount of total sea ice volume loss is generally consistent with the strength of the imposed radiative perturbation, although SW undergoes a greater sea ice volume loss than LW, despite similar changes in Arctic sea ice area (Fig. 1d), which suggests a slightly higher radiative imbalance in the SW experiment than in the LW.

We first focus on the SW experiment and compare its climatological sea ice concentration to the observations (Fig. 2) and the control (supplementary Fig. S2). September sea ice extent decreases all over the Arctic and the Nordic Seas, with the largest sea ice melting occurring around sea ice margins, especially over the shelf area and along the path of the East Greenland Current (Fig. 2d). In March, the area-integrated total sea ice area reduces by less than 10% (Fig. 1d), but there are important spatial changes in the North Atlantic. In particular, the model shows generally reduced sea ice extent in the basins south of Greenland (Fig. 2c), suggesting a weakening of local sea ice formation and sea ice export from the Arctic ocean (supplementary Fig. S3). The reduction of sea ice extent to the northeast of Iceland, which is on the margins of winter sea ice cover in the control climate, indicates a retreat of winter sea ice edge in this region. Meanwhile, a slightly increased sea ice extent is found between the Barents Sea and Norwegian Sea, and within the Irminger Sea. These locations trace the North Atlantic Current, suggesting anomalous cooling along its path. This is in line with the weakened AMOC transport in these experiments (supplementary Fig. S4).

Unquestionably, the initial melting of sea ice is expected to freshen the Arctic. Assuming that the total freshwater from the initial melting in SW is spread evenly over the upper 300 m of the ocean area north of 60°N with a mean salinity of 33 psu, this would give a transient salinity reduction of about 0.2 psu. This effect should be relatively short-lived, probably a few decades long, as the released freshwater will spread laterally and mix with waters below. The actual salinity reduction in the model, however, tells a different

story (Fig. 1c). We observe a fast salinity decrease in the first 10 years followed by a persistent gradual freshening over a century before the system reaches a new equilibrium. While the first 10 years of freshening in SW ($\Delta S = 0.2$ psu) can be largely attributed to the rapid sea ice melting, the final salinity anomaly of about 0.6 psu is greater than the initial sea ice melting could have induced; nor does this anomaly decay with time. What causes this enhanced Arctic freshening?

3.2 Changes in salinity distribution

Figure 3 shows the area-weighted vertical profiles of time-mean salinity and temperature in the Arctic region (north of 60°N). At the end of the simulation, the entire ocean column becomes fresher, even though the freshening is most pronounced in the upper ocean. The temperature profile reveals an increase of maximum temperature in the layer of Atlantic inflow water.

We next examine the spatial patterns of salinity anomalies in the upper ocean (0-300 m) and at mid-depth (300–700 m) during the fast sea ice contraction (the first 15 years), the slow adjusting phase (years 16–80), and the final stage (years 151–200), respectively (Fig. 4 and supplementary Fig. S5). Over this timeframe, the Arctic ocean freshwater content must increase in the upper ocean to reduce its salinity. Indeed, in the first 15 years (Fig. 4a), the freshening mainly occurs in the upper Arctic ocean, with the most significant salinity decrease along the Siberian shelf. Meanwhile, the Nordic Seas and the North Atlantic exhibit increased salinity, particularly in the western part of the Norwegian Sea and south of Greenland, corresponding to the most significant wintertime sea ice retreat (Fig. 2c). Along the mid-layer of 300–700 m, the North Atlantic, the Nordic Seas, and a part of the central Arctic become saltier than the control, despite surface sea ice melting. In the years to follow, the upper layer gets fresher, and freshwater anomalies spread out into the subarctic and mid-latitude North Atlantic (Fig. 4c). Salinity at mid-depths is also generally reduced, but areas south of the Greenland and Norwegian Sea remain saltier both in the upper and mid-depth layers (Fig. 4d). By the end of the simulation, both ocean layers become significantly fresher (Fig. 4e, f).

To determine the origin of the mid-depth anomalous salinity, we examine a latitude-depth transect of zonally-averaged salinity (Fig. 5a-c) and temperature (Fig. 5d-f) anomalies within the $10\text{--}15^\circ\text{W}$ sector (marked by the red dashed line in Fig. 4c). This sector is chosen because it coincides with the path of the East Greenland Current, includes the Greenland-Iceland sill, and is close to the positive upper ocean salinity anomaly northeast of Iceland. During the first 15 years (Fig. 5a, d), significantly saltier and warmer surface water within the Norwegian sea penetrates all the way down to the ocean sill. As discussed above, this surface anomaly is due to the retreat of sea ice cover, which lead to reduced freshwater input and greater ocean exposure to direct solar radiation. Here, salinity effects dominate density anomalies. That reduced sea ice cover can cause surface anomalies to pervade through the water column, which emphasizes the sensitivity of convection to surface buoyancy in this region. This anomalously salty and warm water continues to travel northward into the Greenland Sea and the Arctic ocean after reaching the depth of neutral buoyancy at around 200-500m. A similar effect has been found in recent Arctic observations (Timmermans et al. 2018).

Another segment of salty and warm water comes from the southern boundary at 200-500m depth (Fig. 5b-c, e-f), which represents water inflow from the North Atlantic. This shows a strengthened Arctic circulation that coexists with a weakened AMOC (also found in Bitz et al., 2006). The strengthened salt advection is likely caused by the estuarine circulation response (Stigebrandt 1981; Nummelin et al. 2016; Pemberton and Nilsson 2016; Lambert et al. 2019) as well as changes in gyre circulations (supplementary Fig. S6). This discussion reveals that the mid-layer salty water comes from both surface flux-induced convective overturning and horizontal advection from the North Atlantic.

3.3 Changes in freshwater content, surface freshwater fluxes and ocean circulation

To understand the persistent upper-ocean Arctic freshening, next we calculate the simulated changes in the freshwater content (FWC) of the Arctic region. The liquid FWC with respect to a reference state is defined via ocean salinity as:

$$FWC = \iiint_D^0 (S_{ref} - S(x, y, z)) / S_{ref} dz dy dx,$$

where $S(x, y, z)$ is salinity, S_{ref} is the reference salinity of 34.8 psu, and D is the depth of integration. We consider FWC integrated over the total ocean depth, as well as FWC for the upper 300 m.

Figure 6a shows the time series of the anomalous FWC (in km^3) integrated over the Arctic region (north of 60°N). The total-depth anomalous FWC gradually increases over the first ~ 130 years then stabilizes at $8 \times 10^4 \text{ km}^3$. In the first 30–40 years, the FWC increase primarily occurs within the upper 300 m. In the new quasi-equilibrated state, the anomalous FWC of the upper ocean accounts for nearly 70% of the total FWC change. As part of this FWC increase in the upper ocean, the central Arctic FWC (which includes the Canadian and Eurasian Basins) increases by $5 \times 10^4 \text{ km}^3$ (equivalent to a salinity decrease of 0.7 psu), accounting for about 90% of the total upper ocean FWC increase north of 60°N .

The change of the Arctic ocean FWC can come from surface freshwater fluxes (SFC), convergence of horizontal and vertical advection (ADV), and the diffusion term (DF): $\frac{dFWC}{dt} = \text{SFC} + \text{ADV} + \text{DF}$. As the diffusion term is small, we mainly consider changes of surface freshwater fluxes and convergence of freshwater by advection (Fig. 6b). Immediately after the perturbation initiation, the rapid sea ice melting leads to an increase of surface freshwater flux. This anomalous surface flux slowly abates as the sea ice adjusts towards stabilization. Around year 40, the surface freshwater flux reaches to a balanced state, with an anomalous $\sim 0.03 \text{ Sv}$ freshwater input to the ocean compared to the control. It was found that surface buoyancy anomalies are dominated by net freshwater/salt fluxes induced by sea ice melting and brine rejection (e.g., Fig. 6 in Liu et al., 2018). The anomalous surface freshwater input of 0.03 Sv is therefore the result of the strengthened sea ice seasonal cycle with enhanced summer melting (Fig. 1).

$$\frac{dFWC}{dt}$$

In the first 40 years, the trend of FWC($\frac{dFWC}{dt}$) is almost entirely attributed to surface freshwater fluxes associated with sea ice melting, while the effect of total-depth freshwater transport is small (Fig. 6b). Subsequently, after year 40, the freshwater export by ocean circulation increases and eventually balances the surface freshwater fluxes, leading to a quasi-equilibrium.

To better understand the key processes involved in the FWC increase, we analyze the spatial patterns of surface freshwater flux anomalies (Fig. 7) and ocean circulation (Fig. 8). Annual mean anomalous freshwater fluxes are consistent with the patterns of anomalous upper-ocean salinity (Fig. 4a and 7b). The central Arctic receives a large amount of freshwater from sea ice melting, while the Nordic Seas and regions along the East Greenland Current experience generally reduced surface freshwater input owing to reduced sea ice cover and export. The annual mean pattern is largely dominated by anomalies in summer (Fig. 7c) when sea ice melting is the strongest. In winter (Fig. 7d), the central Arctic shows a reduced freshwater flux. The amplitude of the surface salinity seasonal cycle is consistent with that of the freshwater flux, which scales with the imposed perturbation intensity (Fig. 1f and Fig. 7a).

The large freshwater flux input within the central Arctic co-occurs with the strengthening of the Beaufort Gyre (Fig. 8a, c, e), which increases the storage of the upper ocean freshwater made available by the strong summer sea ice melting (in this case, reducing freshwater export). Meanwhile, the Atlantic subpolar gyre weakens, even though the East Greenland Current and West Greenland Current strengthen (Fig. 8a, c, e). The upper 300 m of the ocean maintain a net freshwater export across 60°N of about 0.01 Sv. Note that the freshwater transport in the North Atlantic sector is small throughout the simulation (Fig. 6c), suggesting that the subpolar Atlantic has a small impact on the Arctic upper-ocean freshwater content, and that the feedback from a weakened AMOC on the Arctic upper-ocean freshening is small (more on this in Sect. 4).

In summary, Arctic sea ice decline generates an imbalance between the surface freshwater flux (due to enhanced seasonal melting of sea ice) and the export of freshwater (by ocean circulation). In the process of adjusting to the new state, freshwater accumulates in the Arctic, reducing the upper-ocean salinity. The sea ice thermodynamic adjustment with seasonal melting and re-freezing, and its interactions with the ocean circulation, is key to the upper-ocean freshening.

We see a general agreement between different numerical experiment; however, we find that the LW experiment has a smaller total sea ice volume reduction but a fresher Arctic at the end of the simulation than in the SW experiment (Fig. 1a-c). It is found that the LW experiment generates stronger net surface freshwater fluxes into the ocean than the SW during the adjustment stage, resulting in a higher freshwater accumulation before a new quasi-equilibrium is reached.

3.4 Arctic ocean freshening and salinity changes in the North Atlantic

In the previous discussion in Sect. 3.2, we found that the enhanced convection in a part of the Norwegian Sea and the region south of Greenland may allow surface salinity anomalies to spread down the water column. We now examine the relevant processes to understand how they impact the upper-ocean freshening in the Arctic and, more generally, the salinity distribution in the Arctic and North Atlantic.

Figure 9a shows changes in the upper-ocean stratification averaged over the last 50 years in the SW experiment, which closely follows changes in surface freshwater fluxes (Fig. 7b). The southwestern corner of the Norwegian Sea and the Labrador Sea south of Greenland show reduced stratification and therefore may be prone to convection. Elsewhere in the Arctic and subarctic North Atlantic stratification increases. In particular, stronger stratification in the eastern North Atlantic is related to the reduction in northward salt transport from the subtropics by the weakened AMOC. The anomalous March mixed layer depth shows generally similar features as the changes in upper-ocean stratification (supplementary Fig. S7). The area to the south of Iceland, which is a major part of the original deep convection zone in the control simulation, experiences a significant shoaling of the mixed layer depth, which reflects the weakening of deep convection, and the AMOC slowdown, caused by fresh and warm anomalies at the ocean surface (Liu et al. 2018). The mixed layer deepens in the Beaufort Gyre region, which is paralleled by increased freshwater storage (Fig. 8).

To understand the salinity changes and related processes, we analyze salinity changes over time in two critical regions with the largest buoyancy loss – the region to the south of Greenland and the southwestern corner of the Norwegian Sea (marked in Fig. 9a). For the south of Greenland (box A, Fig. 9b), the anomalously saline water at the surface is transported down via strong convective events to approximately 1000 m depth, where it combines with the upstream dense water and continues to travel south. Year 10 marks the arrival of meltwater from the Arctic, as the upper 300 m begins to freshen up. The convective activity continues throughout the next ~ 200 years, as can be suggested from the correlation between the mixed layer deepening and high salinity signals in the deeper ocean (Fig. 9b and supplementary Fig. S8). Similar features are also present in the Norwegian Sea (box B, Fig. 9c), where anomalous high salinity is present from 50 m to ~ 1500 m during the first century. Sources of this salinity anomaly include convection, sinking of saltier shelf water due to the stronger winter brine rejection, and advection of the Atlantic water (Fig. 5). This saline water then mainly sinks to the deep ocean while the upper ocean gets fresher.

Note that the Labrador Sea was never a deep-water formation site in the control simulation of this model. Likewise, despite the reduced stratification and deepened mixed layer that allow for episodic convective events during the first decades of the sea ice perturbation experiments, these experiments do not develop sustained deep convection in the Labrador Sea. This contrasts the sea ice perturbation experiments with the higher-resolution model which undergoes activation of deep convection in this region (Sect. 3.5 and Li et al. 2021).

We further examine the temporal evolution of the FWC and freshwater transport in the layer of 700–1100 m north of 60°N (Fig. 9d, e). We find that the FWC has a negative anomaly in the first 30 years, consistent

with the increased salt content (see Figs. 5b and 9b-c). This FWC decrease is concurrent with freshwater import by horizontal advection, suggesting that it is vertical processes that cause the increase of salt content at this depth.

Thus, we find that the strengthened sea ice seasonality and the associated changes in sea ice transport freshen the Arctic upper ocean while making ocean deep layers in the Arctic ocean and subarctic North Atlantic more saline (during the first several decades of the perturbation experiments). This resembles a distillation process that would remove salt from the upper ocean and increase salinity at depth.

The salt accumulated in deeper layers of the subarctic North Atlantic is then advected southward by the Deep Western Boundary Current (DWBC) as seen in a Hovmoller diagram of zonally-averaged anomalous salinity estimated at the typical depths of DWBC (1700–2000 m) in the Atlantic Ocean (Fig. 10a). The most saline water mass, first seen at 55–60°N at year 10, propagates southward into mid-latitudes over the following 40 years. Analyzing area-averaged salinity anomalies at three latitudinal bands (averaged over 40–55°W, 1700–2000 m) along the meridional transport pathway. With time, the subarctic North Atlantic Ocean becomes fresher, while the ocean at lower latitudes becomes more saline. The high to low latitudes salinity contrast is further amplified by the AMOC slowdown and hence the reduced upper-ocean northward transport of saline subtropical waters.

The evolution of depth-integrated ocean salt content further illustrates the process by which salt is taken out of the subarctic ocean (Fig. 10b-e). Positive salt content anomalies evident in the Nordic Seas and in the Labrador Sea during the first decades of the perturbation experiment are gradually transported out of the high-latitudes over approximately 80 years. The pathway of the export is mainly along DWBC (Fig. 10e and supplementary animation). Eventually, a strong negative salinity anomaly develops in the eastern North Atlantic at the latitude of 45°N, resulting largely from the reduced northward transport by the AMOC. These changes together lead to a pronounced freshening in the mid-to-high latitude North Atlantic but increased salinity in the tropical and subtropical ocean (supplementary Fig. S9).

3.5 Results from the higher-resolution model

A persistent freshening of the Arctic is also evident in the SW sea ice decline experiment (Fig. 11) using a higher-resolution CESM configuration (f19_gx1v6) with a nominal 1° ocean horizontal grid spacing; for further model details see Sect. 2. In this model the upper-ocean salinity falls to its minimum around years 20–30 then increases slightly, reaching a new balance with an average salinity reduction of 0.2 psu in the second half of the experiments relative to the Control. The total adjustment timescale is also about 100 years.

The vertical profiles of the Arctic average salinity and temperature in the high-res perturbation experiment share similar features as the low-res model (Fig. 12). However, in the high-res model, the upper ocean freshening is primarily confined to the upper-ocean of the central Arctic, while the Barents Sea, the Nordic Seas and the rest of subarctic Atlantic become more saline by the end of the perturbation simulations (Fig. 13). By comparing the temporal evolution of the Arctic FWC (Fig. 14), we find that the differences in

the responses between the two models are largely attributed to the interplay between freshwater advection and changes in ocean circulation. In particular, the subpolar gyre circulation in the high-res model strengthens and begins to export the anomalous meltwater (Fig. 14b and Fig. 8). By year 30, the freshwater export entirely offsets (and will overwhelm later) the positive local freshwater flux. Around year 30, the AMOC also starts to recover from the initial weakening (supplementary Fig. S4), joining force with the strengthened subpolar (Fig. 8) to import more saline Atlantic water into the Arctic. As a result, the total depth-integrated freshwater content decreases. The upper-ocean salinity increases over the subpolar Atlantic and the Nordic Seas (Fig. 13), due to both decreased surface flux and the increased transport of saline Atlantic water (supplementary Fig. S10). Note that despite the enhanced salinity import, the central Arctic upper ocean still shows persistent freshening.

It is critical that the two models have very different responses in ocean circulation. While the advection from the Atlantic has very little effect on the Arctic upper ocean FWC in the low-res model (Fig. 6c), it is a dominant factor in the high-res model (Fig. 14b-c). In the control climate, the North Atlantic subpolar gyre, the North Atlantic Current and the Norwegian Current are stronger in the high-res model than in the low-res model (Fig. 8b). Salt advection by the North Atlantic Current can therefore have a stronger effect on the Nordic Seas and even the Barents Sea.

In fact, changes in the North Atlantic are an essential component of changes in the AMOC. Accordingly, the AMOC responses are also different between the two models: in the low-res perturbation experiments, the AMOC weakens continuously during the first ~ 100 years, approaching a new quasi-equilibrium; in the high-res model, the AMOC weakens by only 10% during the first 20–30 years, which is followed by a full recovery and a slight overshoot (supplementary Fig. S4). Li et al. (2021) find that the diverging AMOC behaviors in the two models are related to differences in the AMOC stability properties, which are controlled by the model mean states, including the basin-wide mean surface freshwater fluxes.

4. Discussion And Conclusions

Ocean circulation in the Arctic is dominated by thermohaline forcing and winds. Sea ice melting, re-freezing, and southward transport all play an important role in regulating surface buoyancy fluxes in the Arctic. In this modeling study we find that the enhanced sea ice seasonal cycle associated with Arctic sea ice decline results in more sea ice melted locally in the Arctic during summer and less transported southward. The excess surface freshwater gradually accumulates as the ocean circulation adjusts towards a new balance for about 100 years, during which the Beaufort gyre also strengthens, increasing Arctic freshwater storage. At the same time, the reduction of sea ice supply and stronger brine rejection make some of the areas at the margins of sea ice and along the continental shelves more saline, especially during the first several decades. These areas serve to transport the anomalously saline water down to oceanic deeper layers, which occurs despite the overall weakening of deep convection and the AMOC in our experiments. The excess salt is subsequently transported away by the lower (southward) branch of the AMOC. The AMOC slowdown and the associated reduction of northward salt transport lead to a further freshening of the North Atlantic subpolar region (southward of 60°N).

The aforementioned results are obtained in a suite of sea ice decline perturbation experiments using different types and magnitude of forcing within a relatively coarse climate model (CESM1, T31_gx3v7 configuration). However, similar salinity changes and the persistent freshening of the Arctic ocean are also seen in simulations within a higher-resolution model (CESM f19_gx1v6, configuration, with a nominal 1° ocean horizontal grid spacing) supporting the robustness of our results. The freshening in the higher-resolution model is especially pronounced in the upper ocean in the central Arctic. Over the course of the perturbation experiments (200 years), average Arctic upper-ocean salinity decreases to its minimum around year 30, recovers a little, and then maintains a fresher equilibrium state.

In SW experiments, the high-res model produces a similar magnitude of Arctic sea ice decline but exhibits a very different ocean circulation response compared to the low-res model. In particular, the AMOC in the lower resolution model experiences significant and continuous weakening in the first 100 years and approaches a new quasi-equilibrated state. In contrast, in the high-res model the AMOC weakens by less than 10% followed by a full recovery. The causes of these differences are investigated in detail in a complementary study by Li et al. (2021), who argue that the AMOC in the high-res model is overly stable because of a strong negative basin-scale salt-advection feedback related to the overall freshwater budget of the Atlantic basin. This negative feedback leads to a full recovery of the AMOC, which also involves the activation of deep convection in the Labrador Sea.

Differences in the AMOC response affect the strength and structure of the Arctic freshening as well as salinity changes outside the Arctic. The recovery and a slight strengthening of the AMOC in the second half of the high-res experiments, combined with the strengthened subpolar gyre circulation, transports more saline water into the Nordic Seas. Subsequently, the total freshening north of 60°N is weaker in the high-res model than in the low-res. The differences between the two models show that Arctic freshening in a warming climate depends on intricate interactions between sea ice thermodynamic adjustment, ocean stratification and deep convection, as well as the details of Arctic-Atlantic connection through ocean circulation.

Note that the patterns of sea ice reduction in the two models are somewhat different from the observations, despite a realistic reduction of Arctic sea ice extent in the experiments (Fig. 1–2). For example, in the observations winter sea ice loss occurs mostly in the Barents-Kara Seas and the Sea of Okhotsk, and summer sea ice loss is in the central Arctic. By contrast, the largest winter sea ice loss in the low-res SW experiment is in the basins south of Greenland, to the northeast of Iceland and in the Bering Sea, and the largest summer sea ice loss occurs on the margins of sea ice. These differences can be due to the model's representation of climatological sea ice and its interactions with the ocean and the atmosphere boundary. The spatial distribution of sea ice loss can affect freshwater storage and transport and needs to be taken into consideration when interpreting the model results.

The Arctic ocean is expected to freshen in the 21st century – according the Coupled Model Intercomparison Project phase 5 (CMIP5), under the Representative Concentration Pathway 8.5 (RCP8.5) scenario. Arctic Ocean average sea surface salinity is projected to decrease by 1.5 ± 1.1 psu (Shu et al.

2018). The persistent Arctic freshening effect due to the enhanced sea ice seasonal melting, as described in our study, should be a major part of this freshening along with other factors, including the melting of the Greenland ice sheet (Bitz et al. 2006; Shu et al. 2018) and projected increase in precipitation and river run-off in high latitudes (Fischer and Knutti 2015). Thus, this study confirms that the future Arctic will become significantly fresher in years to come.

5. Declarations

- *Acknowledgments:* We are grateful to Wei Liu (University of California Riverside) for making available the model output for analysis. Support from the Yale University High Performance Computing center is also acknowledged.

- *Funding:* This study is supported by grants from NSF (OCE-1756682, OPP-1741847), the ARCHNGE project of the “Make our planet great again” program (CNRS, France), and the Guggenheim fellowship to AVF. H. Li is supported by the Regional and Global Climate Modeling Program (RGCM) of the U.S. Department of Energy's Office of Biological & Environmental Research (BER) via National Science Foundation IA 1844590.

- *Conflicts of interest/Competing interests:* Not Applicable

- *Data, materials, and code availability:* The observational record for sea ice area provided by the National Snow and Ice Data Center (NSIDC) is available at <https://nsidc.org/data/NSIDC-0051/versions/1>. Sea ice volume from Pan-Arctic Ice Ocean Modeling and Assimilation System (PIOMAS) can be accessed at <http://psc.apl.uw.edu/research/projects/arctic-sea-ice-volume-anomaly/data/>. Additional model data and code can be requested from the authors.

- *Author contributions:* H. Li performed the calculations and analysis as well as produced the Figures. Both authors discussed the results and contributed to writing the manuscript. A. V. Fedorov directed this work with contributions from H. Li.

6. References

1. Aagaard K, Carmack EC (1989) The role of sea ice and other fresh water in the Arctic circulation. *Journal of Geophysical Research: Oceans* 94:14485–14498. <https://doi.org/10.1029/JC094iC10p14485>
2. Bamber J, van den Broeke M, Ettema J, et al (2012) Recent large increases in freshwater fluxes from Greenland into the North Atlantic: FRESHWATER INTO THE NORTH ATLANTIC. *Geophys Res Lett* 39:n/a-n/a. <https://doi.org/10.1029/2012GL052552>
3. Bitz CM, Gent PR, Woodgate RA, et al (2006) The Influence of Sea Ice on Ocean Heat Uptake in Response to Increasing CO₂. *J Climate* 19:2437–2450. <https://doi.org/10.1175/JCLI3756.1>

4. Blackport R, Kushner PJ (2016) The Transient and Equilibrium Climate Response to Rapid Summertime Sea Ice Loss in CCSM4. *Journal of Climate* 29:401–417. <https://doi.org/10.1175/JCLI-D-15-0284.1>
5. Cavalieri DJ, Parkinson CL (2008) Antarctic sea ice variability and trends, 1979–2006. *J Geophys Res* 113:C07004. <https://doi.org/10.1029/2007JC004564>
6. Cohen J, Screen JA, Furtado JC, et al (2014) Recent Arctic amplification and extreme mid-latitude weather. *Nature Geoscience* 7:627–637. <https://doi.org/10.1038/ngeo2234>
7. Cornish SB, Kostov Y, Johnson HL, Lique C (2020) Response of Arctic Freshwater to the Arctic Oscillation in Coupled Climate Models. *J Climate* 33:2533–2555. <https://doi.org/10.1175/JCLI-D-19-0685.1>
8. Deser C, Tomas RA, Sun L (2015) The Role of Ocean–Atmosphere Coupling in the Zonal-Mean Atmospheric Response to Arctic Sea Ice Loss. *Journal of Climate* 28:2168–2186. <https://doi.org/10.1175/JCLI-D-14-00325.1>
9. Eisenman I, Schneider T, Battisti DS, Bitz CM (2011) Consistent Changes in the Sea Ice Seasonal Cycle in Response to Global Warming. *Journal of Climate* 24:5325–5335. <https://doi.org/10.1175/2011JCLI4051.1>
10. Fischer EM, Knutti R (2015) Anthropogenic contribution to global occurrence of heavy-precipitation and high-temperature extremes. *Nature Clim Change* 5:560–564. <https://doi.org/10.1038/nclimate2617>
11. Goldstein MA, Lynch AH, Zsom A, et al (2018) The step-like evolution of Arctic open water. *Sci Rep* 8:16902. <https://doi.org/10.1038/s41598-018-35064-5>
12. Haine TWN, Curry B, Gerdes R, et al (2015) Arctic freshwater export: Status, mechanisms, and prospects. *Global and Planetary Change* 125:13–35. <https://doi.org/10.1016/j.gloplacha.2014.11.013>
13. Holland MM, Bailey DA, Briegleb BP, et al (2012) Improved Sea Ice Shortwave Radiation Physics in CCSM4: The Impact of Melt Ponds and Aerosols on Arctic Sea Ice*. *Journal of Climate* 25:1413–1430. <https://doi.org/10.1175/JCLI-D-11-00078.1>
14. Johnson HL, Cornish SB, Kostov Y, et al (2018) Arctic Ocean Freshwater Content and Its Decadal Memory of Sea-Level Pressure. *Geophysical Research Letters* 45:4991–5001. <https://doi.org/10.1029/2017GL076870>
15. Kwok R, Rothrock DA (2009) Decline in Arctic sea ice thickness from submarine and ICESat records: 1958–2008: ARCTIC SEA ICE THICKNESS. *Geophys Res Lett* 36:n/a-n/a. <https://doi.org/10.1029/2009GL039035>
16. Lambert E, Nummelin A, Pemberton P, Ilıcak M (2019) Tracing the Imprint of River Runoff Variability on Arctic Water Mass Transformation. *Journal of Geophysical Research: Oceans* 124:302–319. <https://doi.org/10.1029/2017JC013704>
17. Li H, Fedorov A, Liu W (2021) AMOC Stability and Diverging Response to Arctic Sea Ice Decline in Two Climate Models. *Journal of Climate* 34:5443–5460. <https://doi.org/10.1175/JCLI-D-20-0572.1>

18. Liu W, Fedorov A, Sévellec F (2018) The mechanisms of the Atlantic Meridional Overturning Circulation slowdown induced by Arctic sea ice decline. *Journal of Climate*. <https://doi.org/10.1175/JCLI-D-18-0231.1>
19. Liu W, Fedorov AV (2019) Global Impacts of Arctic Sea Ice Loss Mediated by the Atlantic Meridional Overturning Circulation. *Geophys Res Lett* 46:944–952. <https://doi.org/10.1029/2018GL080602>
20. Neale RB, Gettelman A, Park S, et al (2012) Description of the NCAR Community Atmosphere Model (CAM 5.0), Tech. Note NCAR/TN-486+STR, Natl. Cent. for Atmos. In: 6of7 ZHAO ET AL.: AEROSOL FIE SIMULATED BY CAMS L08806. pp 2009–038451
21. Nummelin A, Ilicak M, Li C, Smedsrud LH (2016) Consequences of future increased Arctic runoff on Arctic Ocean stratification, circulation, and sea ice cover. *Journal of Geophysical Research: Oceans* 121:617–637. <https://doi.org/10.1002/2015JC011156>
22. Oudar T, Sanchez-Gomez E, Chauvin F, et al (2017) Respective roles of direct GHG radiative forcing and induced Arctic sea ice loss on the Northern Hemisphere atmospheric circulation. *Clim Dyn* 49:3693–3713. <https://doi.org/10.1007/s00382-017-3541-0>
23. Pemberton P, Nilsson J (2016) The response of the central Arctic Ocean stratification to freshwater perturbations. *Journal of Geophysical Research: Oceans* 121:792–817. <https://doi.org/10.1002/2015JC011003>
24. Proshutinsky A, Krishfield R, Timmermans M-L, et al (2009) Beaufort Gyre freshwater reservoir: State and variability from observations. *Journal of Geophysical Research: Oceans* 114:. <https://doi.org/10.1029/2008JC005104>
25. Rabe B, Karcher M, Kauker F, et al (2014) Arctic Ocean basin liquid freshwater storage trend 1992–2012. *Geophysical Research Letters* 41:961–968. <https://doi.org/10.1002/2013GL058121>
26. Schweiger A, Lindsay R, Zhang J, et al (2011) Uncertainty in modeled Arctic sea ice volume. *J Geophys Res* 116:C00D06. <https://doi.org/10.1029/2011JC007084>
27. Scinocca JF, Reader MC, Plummer DA, et al (2009) Impact of sudden Arctic sea-ice loss on stratospheric polar ozone recovery. *Geophys Res Lett* 36:L24701. <https://doi.org/10.1029/2009GL041239>
28. Serreze M, Barrett A, Stroeve J, et al (2009) The emergence of surface-based Arctic amplification. *The Cryosphere* 3:11–19. <https://doi.org/10.5194/tc-3-11-2009>
29. Serreze MC, Barrett AP, Slater AG, et al (2006) The large-scale freshwater cycle of the Arctic. *J Geophys Res* 111:C11010. <https://doi.org/10.1029/2005JC003424>
30. Sévellec F, Fedorov AV, Liu W (2017) Arctic sea-ice decline weakens the Atlantic Meridional Overturning Circulation. *Nature Clim Change* 7:604–610. <https://doi.org/10.1038/nclimate3353>
31. Shu Q, Qiao F, Song Z, et al (2018) Projected freshening of the Arctic Ocean in the 21st century. *J Geophys Res Oceans* 2018JC014036. <https://doi.org/10.1029/2018JC014036>

32. Smith R, Jones P, Briegleb B, et al (2010) The parallel ocean program (POP) reference manual ocean component of the community climate system model (CCSM) and community earth system model (CESM). Rep LAUR-01853 141:
33. Stigebrandt A (1981) A Model for the Thickness and Salinity of the Upper Layer in the Arctic Ocean and the Relationship between the Ice Thickness and Some External Parameters. *J Phys Oceanogr* 11:1407–1422. [https://doi.org/10.1175/1520-0485\(1981\)011<1407:AMFTTA>2.0.CO;2](https://doi.org/10.1175/1520-0485(1981)011<1407:AMFTTA>2.0.CO;2)
34. Stroeve J, Holland MM, Meier W, et al (2007) Arctic sea ice decline: Faster than forecast: ARCTIC ICE LOSS-FASTER THAN FORECAST. *Geophys Res Lett* 34:. <https://doi.org/10.1029/2007GL029703>
35. Sun L, Alexander M, Deser C (2018) Evolution of the Global Coupled Climate Response to Arctic Sea Ice Loss during 1990–2090 and Its Contribution to Climate Change. *J Climate* 31:7823–7843. <https://doi.org/10.1175/JCLI-D-18-0134.1>
36. Timmermans M-L, Toole J, Krishfield R (2018) Warming of the interior Arctic Ocean linked to sea ice losses at the basin margins. *Sci Adv* 4:eaat6773. <https://doi.org/10.1126/sciadv.aat6773>
37. Uttal T, Curry JA, McPhee MG, et al (2002) Surface Heat Budget of the Arctic Ocean. *Bull Amer Meteor Soc* 83:255–276. [https://doi.org/10.1175/1520-0477\(2002\)083<0255:SHBOTA>2.3.CO;2](https://doi.org/10.1175/1520-0477(2002)083<0255:SHBOTA>2.3.CO;2)
38. Wang K, Deser C, Sun L, Tomas RA (2018a) Fast Response of the Tropics to an Abrupt Loss of Arctic Sea Ice via Ocean Dynamics. *Geophysical Research Letters* 45:4264–4272. <https://doi.org/10.1029/2018GL077325>
39. Wang Q, Wekerle C, Danilov S, et al (2018b) Arctic Sea Ice Decline Significantly Contributed to the Unprecedented Liquid Freshwater Accumulation in the Beaufort Gyre of the Arctic Ocean. *Geophys Res Lett* 45:4956–4964. <https://doi.org/10.1029/2018GL077901>
40. Winton M (2006) Amplified Arctic climate change: What does surface albedo feedback have to do with it? *Geophysical Research Letters* 33:. <https://doi.org/10.1029/2005GL025244>
41. Woodgate RA, Weingartner TJ, Lindsay R (2012) Observed increases in Bering Strait oceanic fluxes from the Pacific to the Arctic from 2001 to 2011 and their impacts on the Arctic Ocean water column. *Geophys Res Lett* 39:2012GL054092. <https://doi.org/10.1029/2012GL054092>
42. Zhang J, Rothrock DA (2003) Modeling Global Sea Ice with a Thickness and Enthalpy Distribution Model in Generalized Curvilinear Coordinates. *MONTHLY WEATHER REVIEW* 131:17

Figures

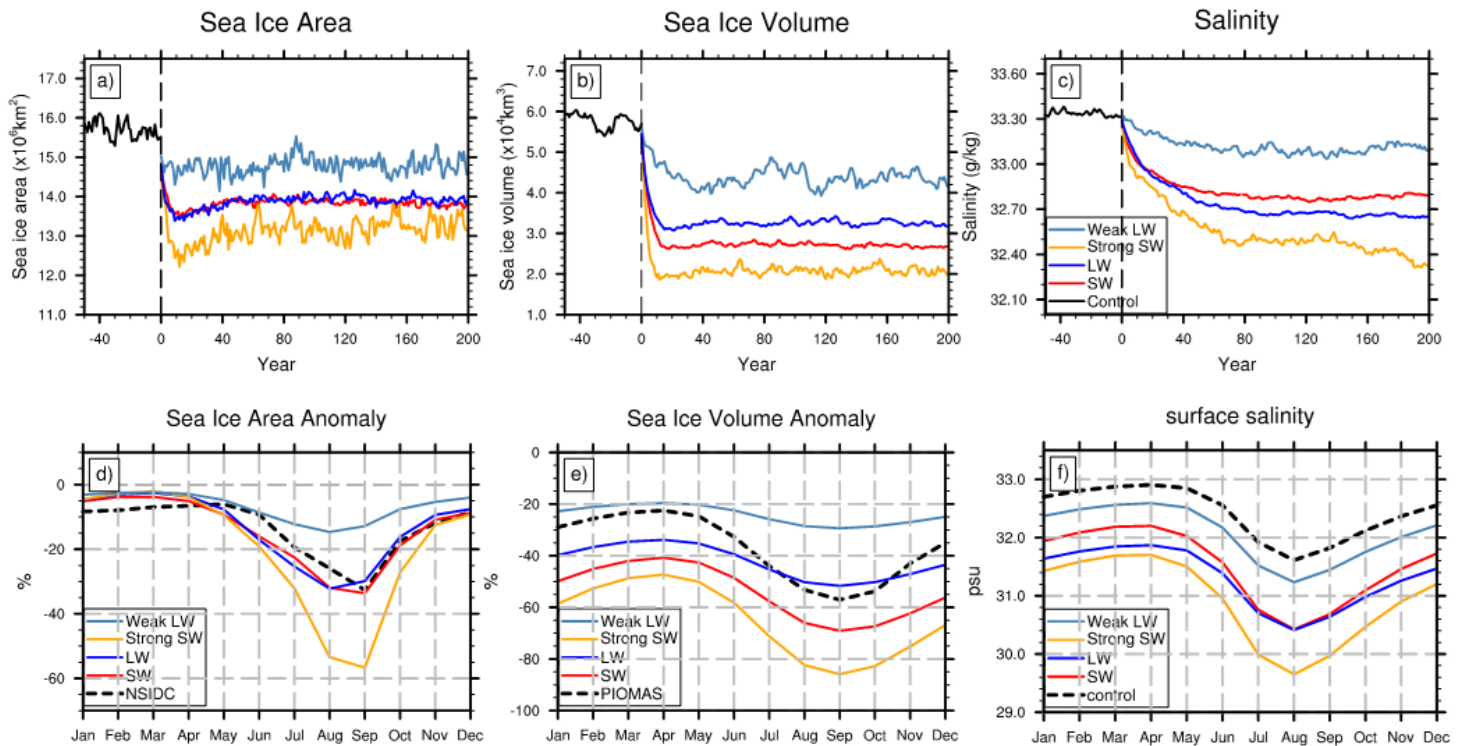


Figure 1

Modeled and observed changes in Arctic sea ice area, sea ice volume, and upper ocean salinity. Time series of (a) sea ice area (unit: $1 \times 10^6 \text{ km}^2$), (b) sea ice volume (unit: $1 \times 10^4 \text{ km}^3$), and (c) salinity (unit: g/kg) in the upper 300 m ocean averaged north of 60°N in the control (black) and the perturbation experiments: weak-LW (light blue), LW (blue), SW (red), and strong-SW (orange). (d) Relative loss (in %) of Arctic monthly-mean sea ice area in the observations (black dashed line) and the perturbation experiments (color lines). (e) As in panel (d) but for sea ice volume. (f) Monthly-mean surface salinity averaged over the ocean area poleward of 60°N in the control (black solid line) and perturbation experiments. The observed anomalies are defined as the mean difference between the periods of 2005-2014 and 1979-1988, whereas model anomalies are calculated as the mean difference between the last 50 years of each simulation and the last 50 years of the control. The perturbation experiments are described in Section 2 of the paper. Shading in the top panels indicates ensemble spread when available.

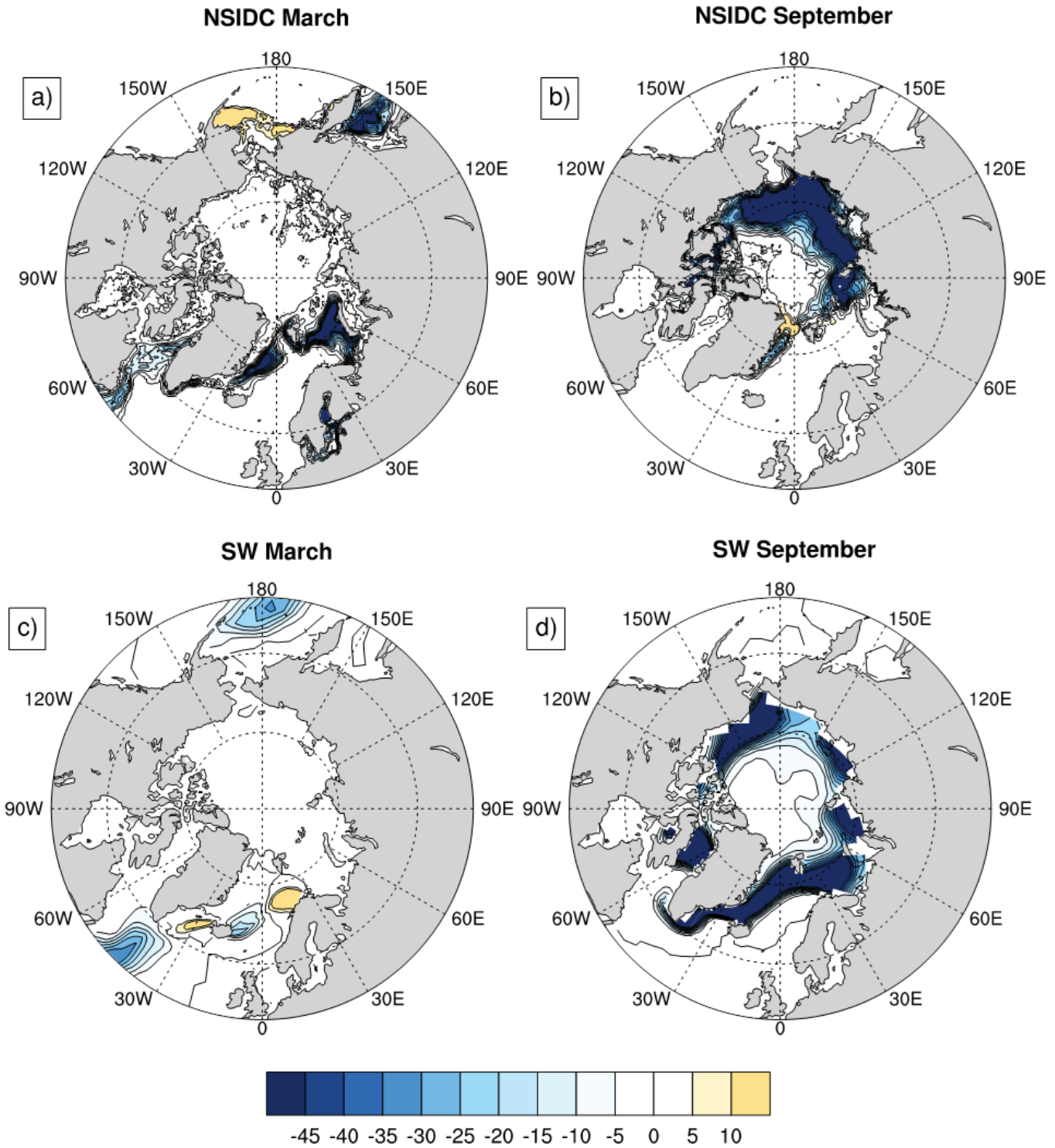


Figure 2

Comparison of modeled and observed sea ice concentration anomalies in March and September. Average sea ice concentration anomalies in March (left) and September (right) for (a, b) the NSIDC observations and (c, d) the SW experiment. The observed anomalies are defined as the mean difference between the periods of 2005-2014 and 1979-1988, whereas model anomalies are calculated as the mean difference between the last 50 years of each simulation and the last 50 years of the control experiment. Note: The

designations employed and the presentation of the material on this map do not imply the expression of any opinion whatsoever on the part of Research Square concerning the legal status of any country, territory, city or area or of its authorities, or concerning the delimitation of its frontiers or boundaries. This map has been provided by the authors.

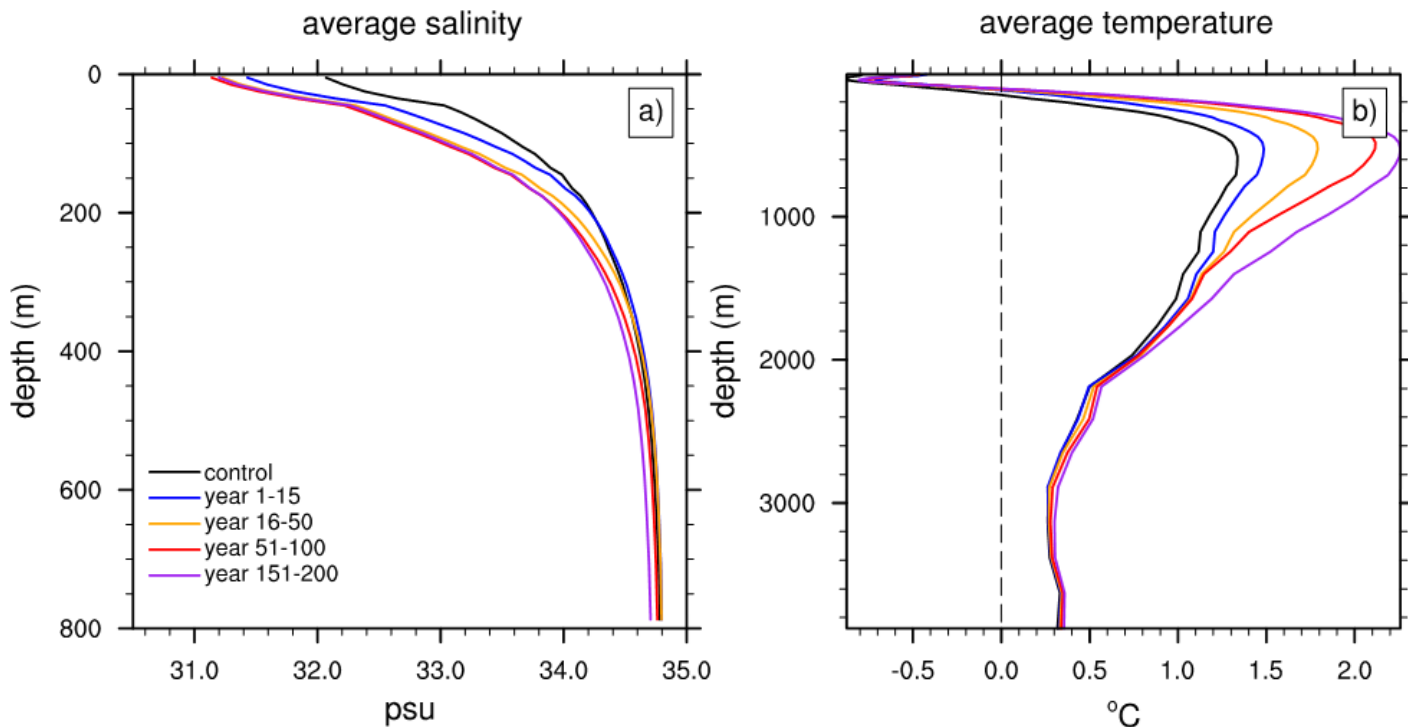


Figure 3

Vertical distributions of salinity and temperature. Vertical profiles of ocean (a) salinity (unit: g/kg) and (b) temperature (unit: °C) averaged for the region north of 60° N and for years 1-15 (blue), years 16-50 (orange), years 51-100 (red), and years 151-200 (purple) of the low-res SW experiment as compared to the control experiment (black).

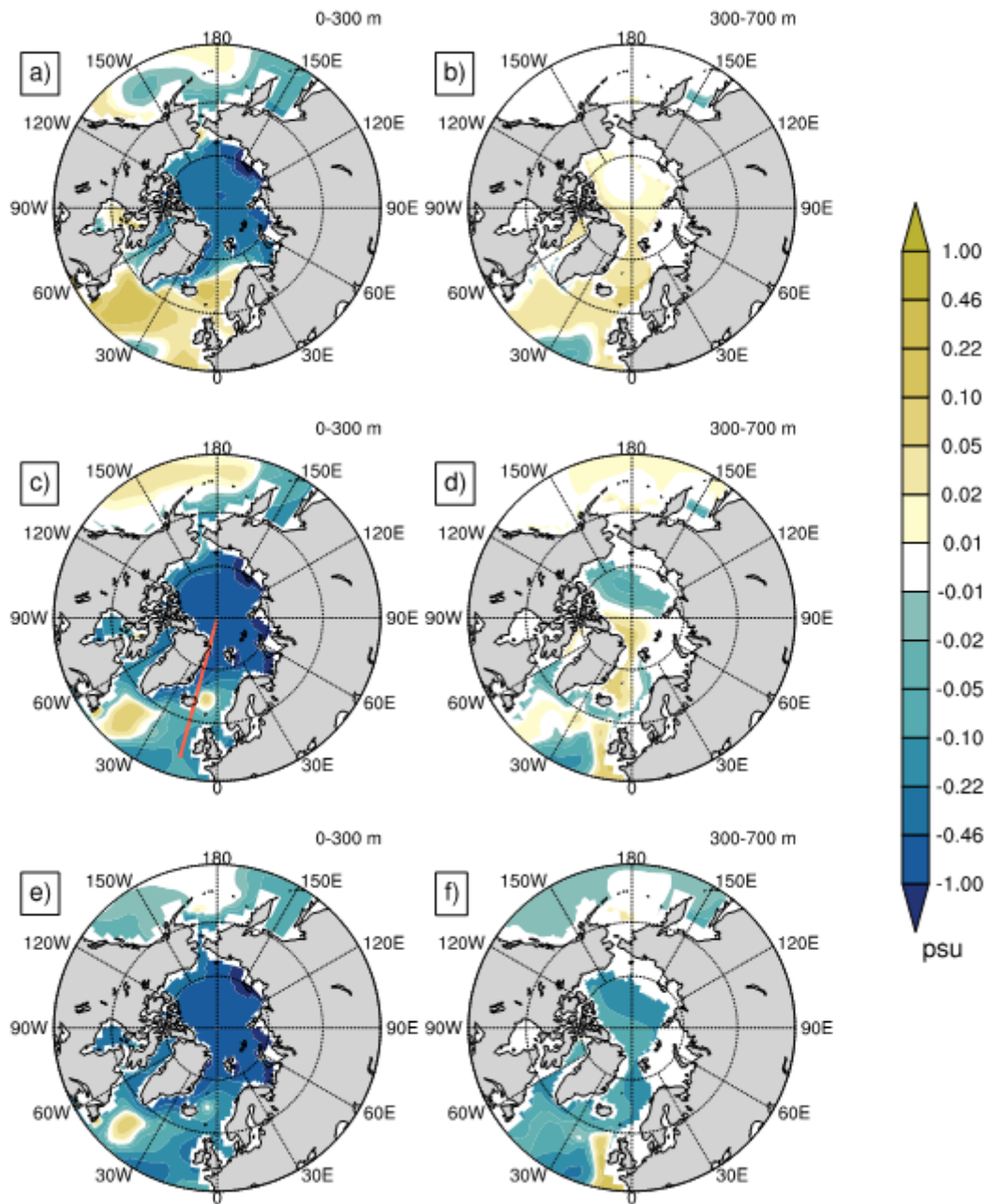


Figure 4

Salinity response to the imposed Arctic sea ice decline in the SW experiment. Salinity anomalies (unit: g/kg) averaged (a, c, e) in the upper 300 m and (b, d, f) in the ocean mid-layer 300-700 m during the initial sea ice contraction (years 1-15, top row), the subsequent slow adjustment (years 16-80, second row), and the final equilibrated stage (years 151-200, bottom row). The red line in panel (c) marks the general location of the 10° - 15° W sector used later in Fig. 5 to analyze latitude-depth transects connecting the North Atlantic and the Arctic oceans. Note: The designations employed and the presentation of the material on this map do not imply the expression of any opinion whatsoever on the part of Research Square concerning the legal status of any country, territory, city or area or of its authorities, or concerning the delimitation of its frontiers or boundaries. This map has been provided by the authors.

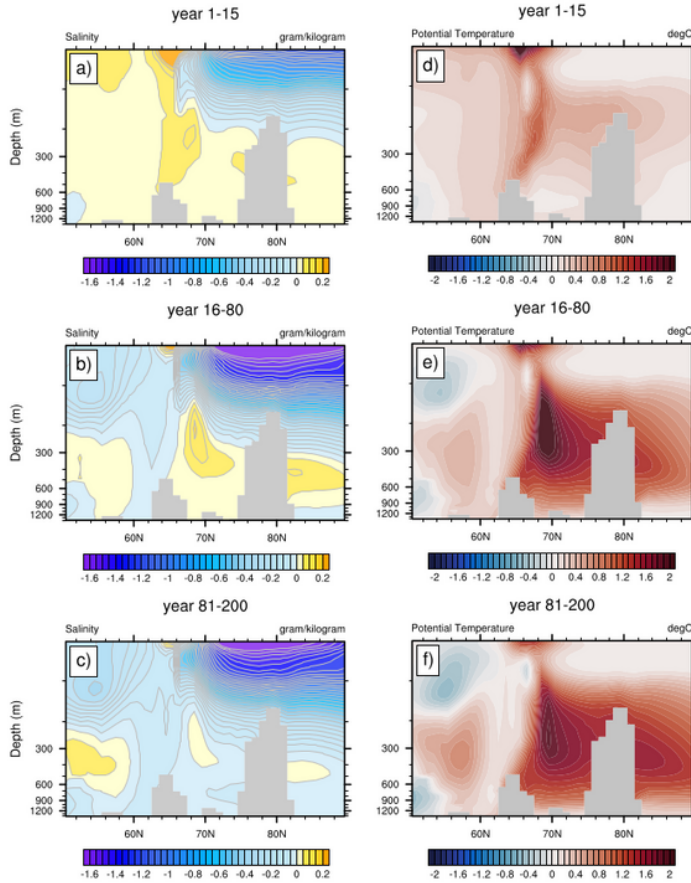


Figure 5

Latitude-depth transects of salinity and temperature anomalies. Zonally-averaged (a-c) salinity and (d-f) temperature anomalies within the 10° - 15° W sector (marked in Fig. 4c) during the initial sea ice loss (years 1-15, top row), the subsequent slow adjustment (years 16-80, second row), and towards the final equilibrated stage (years 81-200, bottom row). Salinity in the units of g/kg, temperature in $^{\circ}$ C. Note that salinity anomalies below 300 m are partially density-compensated by temperature.

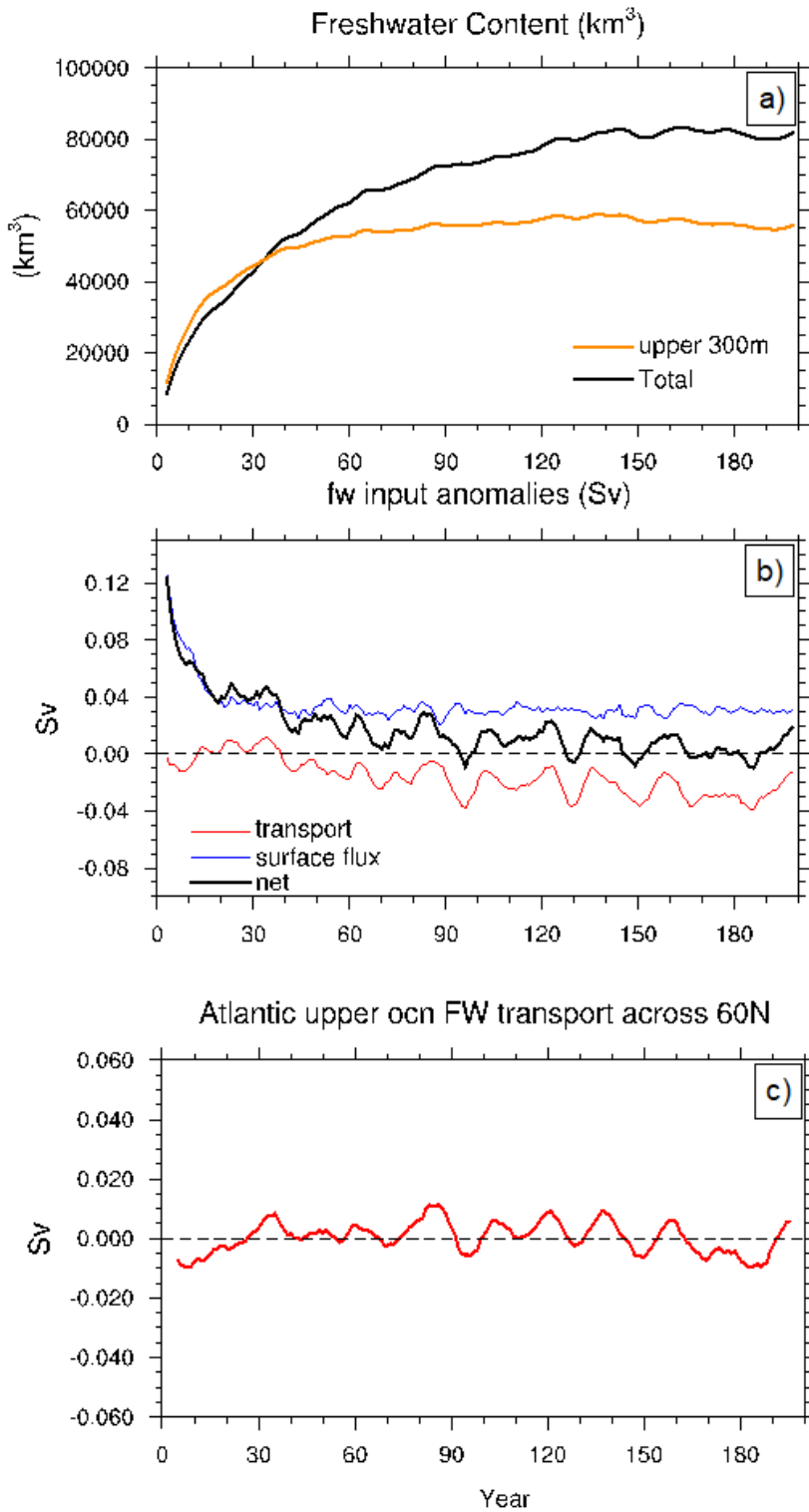


Figure 6

Time series of anomalous freshwater content, surface freshwater fluxes, and freshwater transport. (a) Time series of anomalous freshwater content (unit: km³) north of 60°N, integrated over the total ocean depth (black) and the upper 300 m (orange), respectively and estimated from salinity anomalies (see section 3.3). (b) Anomalies in net surface freshwater flux in the Arctic (north of 60°N) (blue, unit: Sv), total-depth freshwater convergence by advection across 60°N (red, unit: Sv, positive means convergence

of freshwater) and the net freshwater rate of change in the Arctic (i.e., the sum of the aforementioned two terms) (black, unit: Sv). (c) Anomalous upper-ocean (0-300 m) freshwater transport (unit: Sv) across 60°N in the North Atlantic. Positive values indicate anomalous freshwater convergence north of 60°N. Shadings represent the ensemble spread. For the low-res SW experiment. The generally positive net freshwater rate of change (black line in panel b) indicates that the entire Arctic is freshening over the course of the experiment.

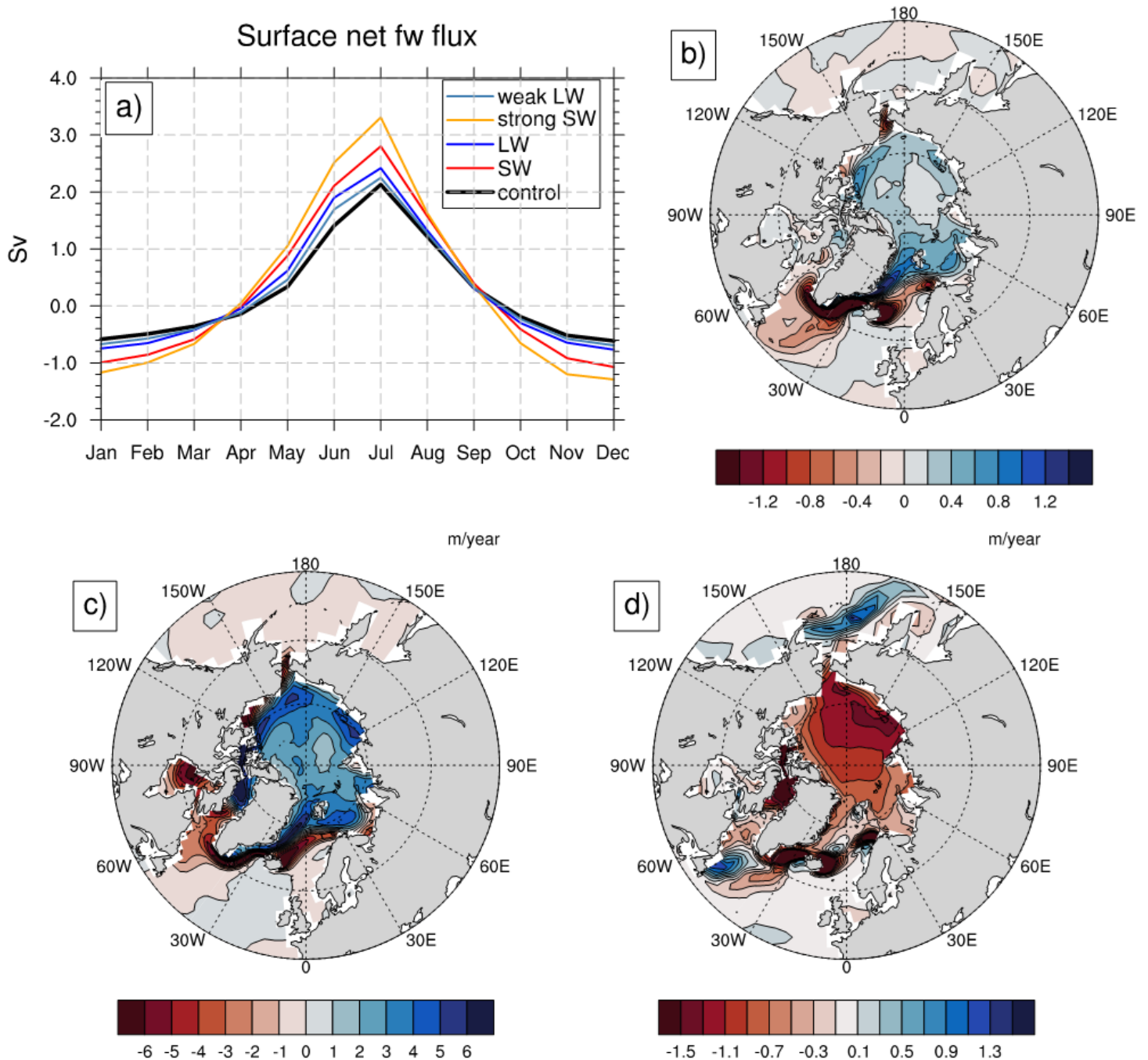


Figure 7

Surface freshwater flux anomalies. (a) Seasonality of net surface freshwater fluxes integrated over the Arctic (unit: Sv) in the control (black) and in the weak-LW (light blue), LW (blue), SW (red), and strong-SW

(orange) experiments. Anomalous surface freshwater fluxes (unit: m/year) in the SW experiment: (b) annual mean, and during (c) summer (July), and (d) winter (January). In the perturbation experiments the fluxes are averaged over the last 50 years. Note: The designations employed and the presentation of the material on this map do not imply the expression of any opinion whatsoever on the part of Research Square concerning the legal status of any country, territory, city or area or of its authorities, or concerning the delimitation of its frontiers or boundaries. This map has been provided by the authors.

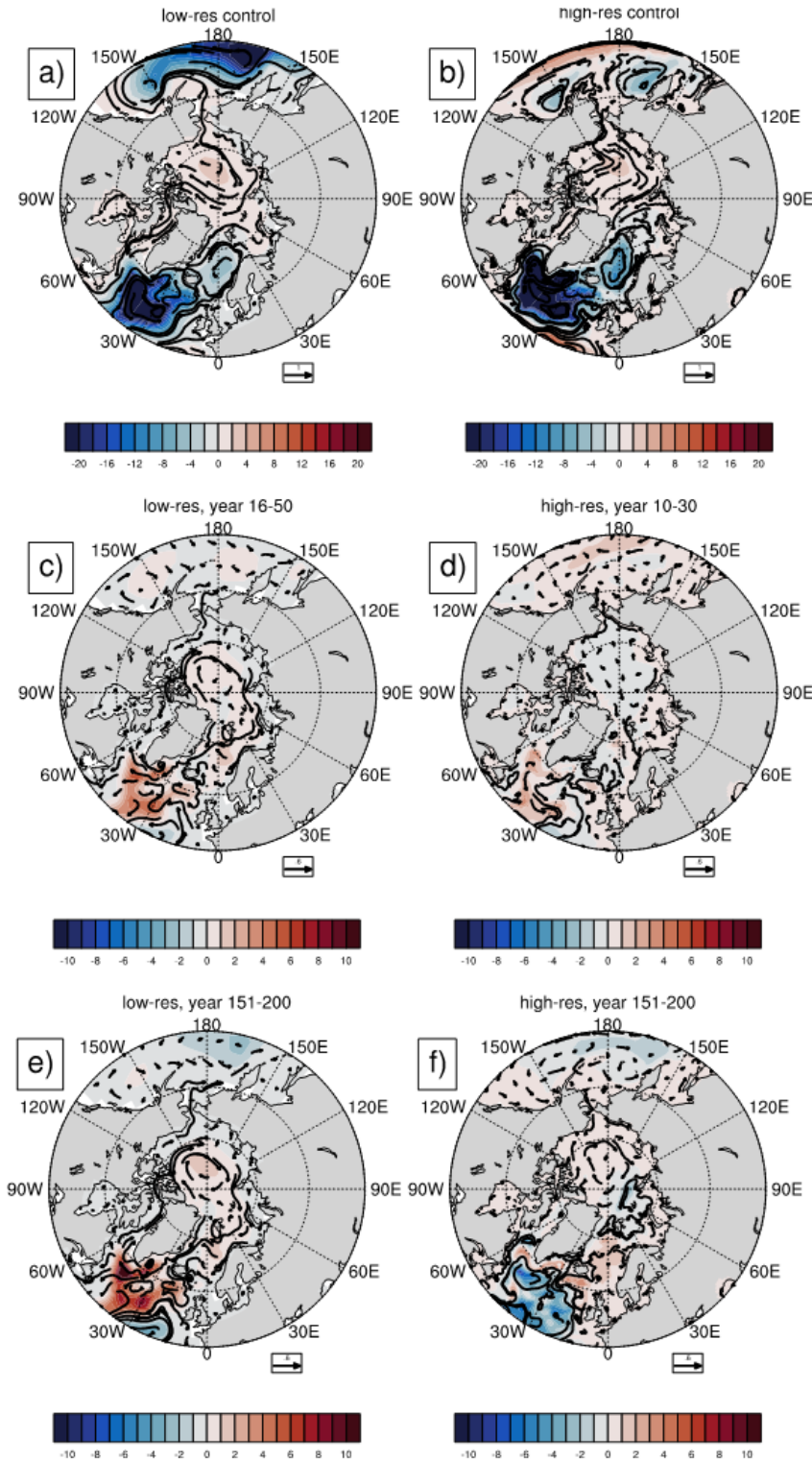


Figure 8

Changes of upper-ocean circulation. Barotropic stream function (color shading, unit: Sv) overlaid with near surface current speed (averaged over 0-100 m) in (a, b) the control experiment, and their anomalies (c, d) during the adjustment period (years 16-50 for the low-resolution and years 10-30 for the high-resolution model) and (e, f) at the end of the SW experiment. The unit arrows for the current speed correspond to 0.6 cm/s. Left: the low-res model. Right: the high-res model. Note the strengthening of the Beaufort gyre in both models especially pronounced by the end of perturbation experiments. In contrast, the subpolar gyre strengthens in the high-resolution model, but weakens in the low-res, which is consistent with the AMOC changes. Note: The designations employed and the presentation of the material on this map do not imply the expression of any opinion whatsoever on the part of Research Square concerning the legal status of any country, territory, city or area or of its authorities, or concerning the delimitation of its frontiers or boundaries. This map has been provided by the authors.

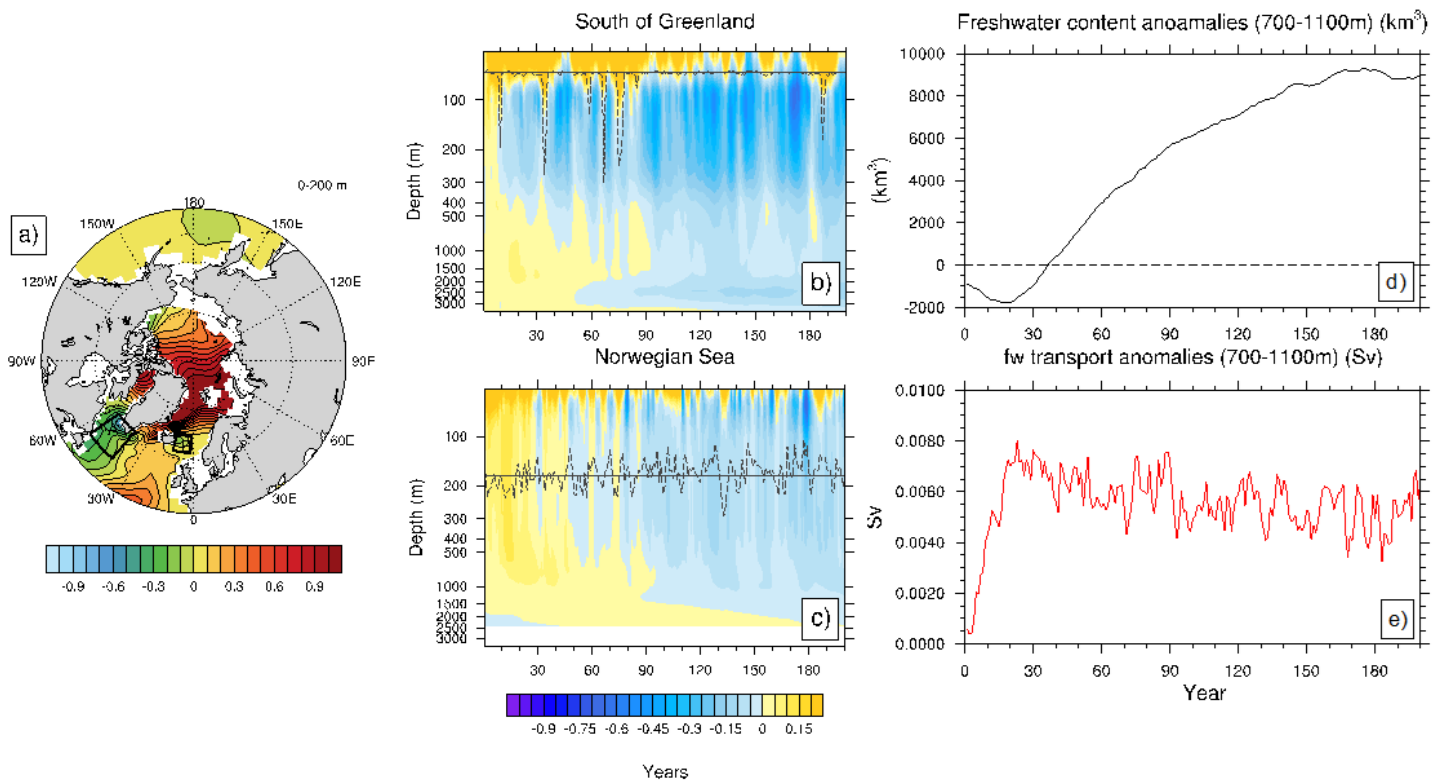


Figure 9

(a) Anomalous upper-ocean stratification averaged over the last 50 years of the SW simulation, which is defined as potential density difference between a 200 m depth and the surface (200 m minus surface). (b, c) Salinity anomalies (unit: g/kg) as a function of ocean depth and time at two locations with reduced stratification as indicated by black boxes in panel a – the region south of Greenland including the Labrador Sea and a patch of the Norwegian Sea east of Iceland. The black dashed lines show the time series of maximum mixed layer depth in the corresponding region, indicative of convection anomalies. Stronger vertical transport of surface salinity anomalies coincides with strong convective events. (d) Time series of anomalous ocean freshwater content (unit: km³) integrated north of 60°N for the layer 700 -1100 m, and (e) total northward freshwater transport (unit: Sv) across 60°N for the layer 700 -1100 m. Positive values indicate anomalous freshwater convergence north of 60°N within this layer. Anomalous

freshwater content is based on salinity anomalies (see section 3.3). Note: The designations employed and the presentation of the material on this map do not imply the expression of any opinion whatsoever on the part of Research Square concerning the legal status of any country, territory, city or area or of its authorities, or concerning the delimitation of its frontiers or boundaries. This map has been provided by the authors.

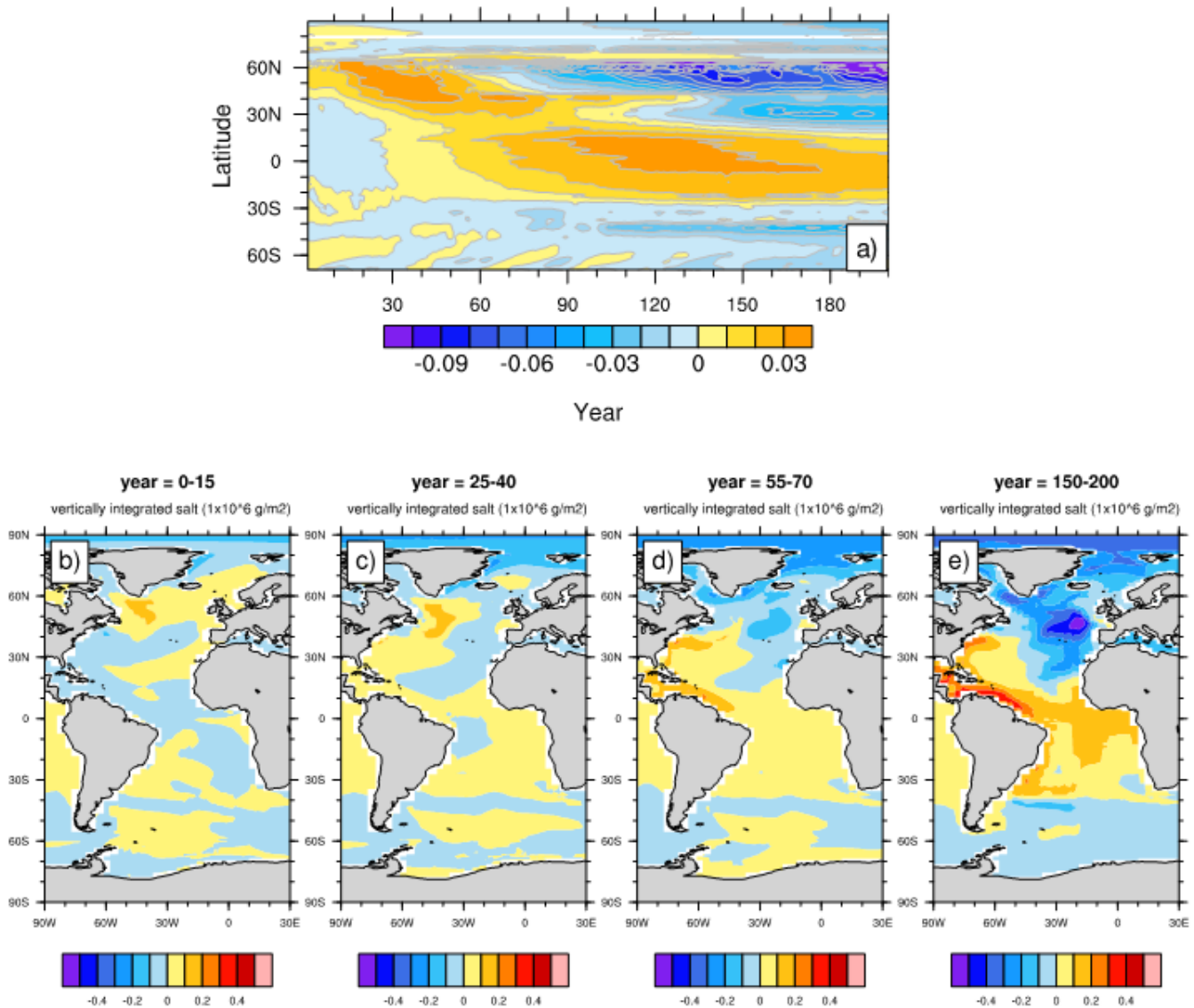


Figure 10

(a) A latitude-time Hovmoller diagram of deep ocean salinity anomalies (unit: g/kg) averaged between 1700-2000 m depths. Snapshots of column-integrated ocean salt content (in 1×10^6 g/m²) averaged for (b) years 1-15, (c) years 25-40, (d) years 55-70, and (e) years 150-200 for the low-res SW experiment. Note the coherent southward propagation of salinity anomalies and the freshening of the Arctic followed by the freshening of the subpolar and mid-latitude North Atlantic. The latter changes are largely caused by the AMOC slowdown. The southward-propagating salinity anomalies follow the path of the Deep Western Boundary Current. Note: The designations employed and the presentation of the material on this map do not imply the expression of any opinion whatsoever on the part of Research Square concerning the legal

status of any country, territory, city or area or of its authorities, or concerning the delimitation of its frontiers or boundaries. This map has been provided by the authors.

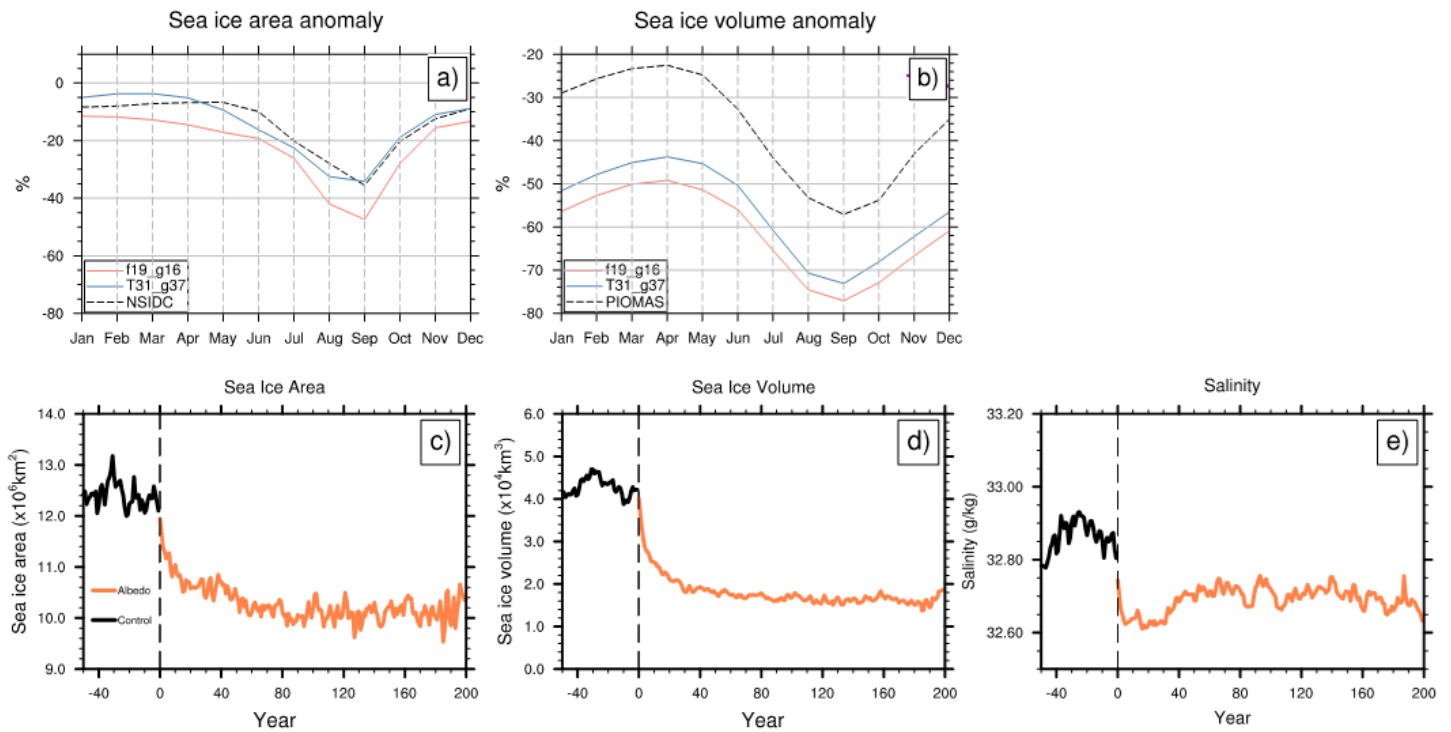


Figure 11

Arctic sea ice and upper ocean salinity in the high-res simulation. Relative loss (in %) of Arctic monthly-mean (a) sea ice area anomalies and (b) sea ice volume anomalies in the observations (black), the SW experiment of the low-resolution model (light blue), and the high-resolution simulation (salmon pink). The anomalies in the observations are defined as the mean difference between the periods of 2005-2014 and 1979-1988. The model anomalies are calculated as the mean difference between the last 50 years of each simulation and the last 50 years of their respective control. Time series of (c) sea ice area (unit: $1 \times 10^6 \text{ km}^2$), (d) sea ice volume (unit: $1 \times 10^4 \text{ km}^3$) and (e) average upper ocean salinity (0-300 m, unit: g/kg) in the control (black) and SW experiment of the high-resolution simulation. Salinity is averaged poleward of 60°N .

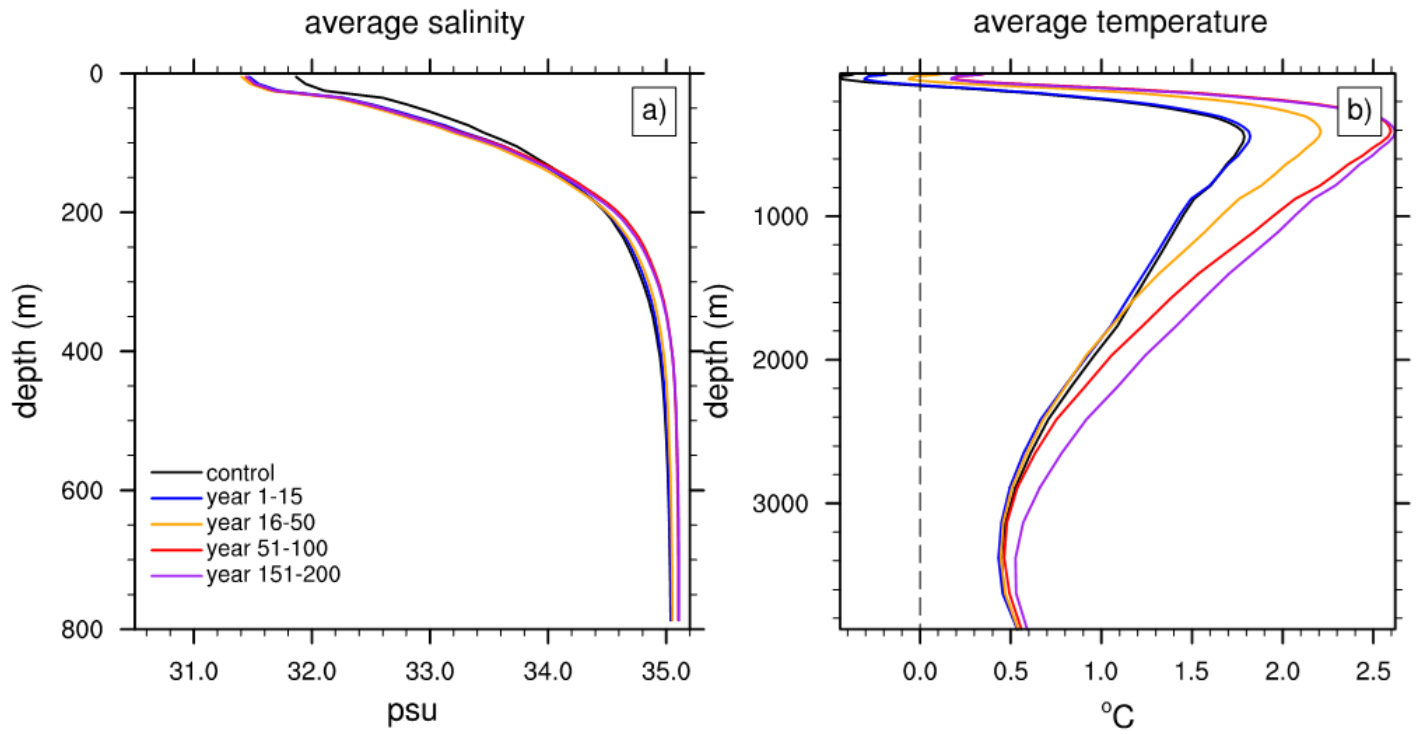


Figure 12

As in Figure 3 but for the profiles of (a) salinity (unit: g/kg) and (b) temperature (unit: °C) simulated in the higher-resolution model. In contrast to the low-resolution model, here the freshening is confined to the Arctic upper ocean.

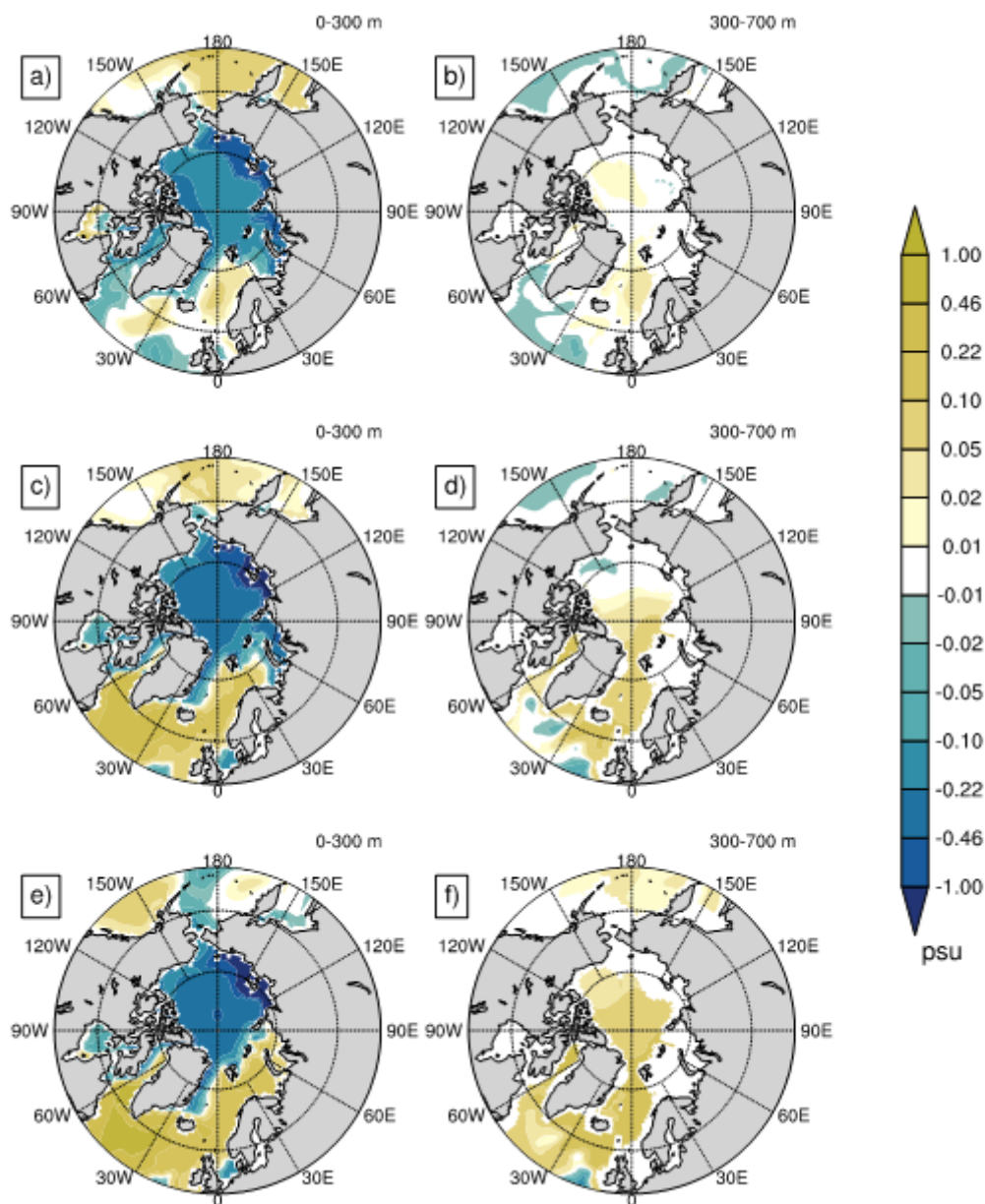


Figure 13

As in Figure 4, but for salinity anomalies simulated in the high-res model. In contrast to the low-resolution model, here the ocean freshening is confined to the Arctic upper ocean while the Nordic Seas and eventually the Barents Sea become more saline. Note: The designations employed and the presentation of the material on this map do not imply the expression of any opinion whatsoever on the part of Research Square concerning the legal status of any country, territory, city or area or of its authorities, or concerning the delimitation of its frontiers or boundaries. This map has been provided by the authors.

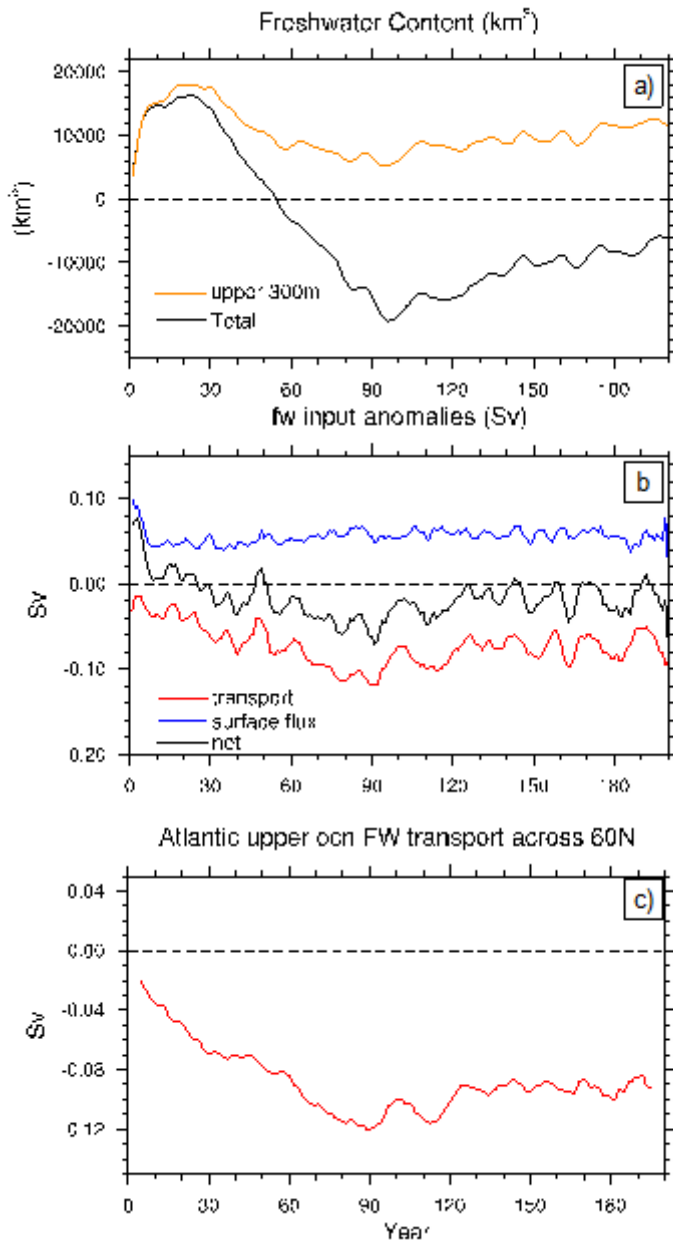


Figure 14

As in Figure 6, but for the high-res model. The slightly negative net freshwater rate of change (black line in panel b) indicates that the Arctic as a whole is losing freshwater, even though the upper-ocean Arctic remains anomalously fresh.

Supplementary Files

This is a list of supplementary files associated with this preprint. Click to download.

- [ArcticFresheningSupplementaryFigures0326.pdf](#)
- [saltlatlonpatternintegrated.gif](#)